Reprinted from *J. Mol. Biol.* (1992) **226**, 169–184

Low Resolution Structure of Microtubules in Solution

Synchrotron X-ray Scattering and Electron Microscopy of Taxol-induced Microtubules Assembled from Purified Tubulin in Comparison with Glycerol and MAP-induced Microtubules

J. M. Andreu, J. Bordas, J. F. Diaz, J. García de Ancos
R. Gil, F. J. Medrano, E. Nogales, E. Pantos
and E. Towns-Andrews

J. Mol. Biol. (1992) **226**, 169–184

Low Resolution Structure of Microtubules in Solution

Synchrotron X-ray Scattering and Electron Microscopy of Taxol-induced Microtubules Assembled from Purified Tubulin in Comparison with Glycerol and MAP-induced Microtubules

J. M. Andreu[1], J. Bordas[2], J. F. Diaz[1], J. García de Ancos[1] R. Gil[1], F. J. Medrano[1,2], E. Nogales[2], E. Pantos[2] and E. Towns-Andrews[2]

[1]*Centro de Investigaciones Biológicas, C.S.I.C. Velázquez 144, 28006 Madrid, Spain*

[2]*S.E.R.C. Daresbury Laboratory Warrington WA4 4AD, U.K.*

(Received 31 May 1991; accepted 13 March 1992)

The structure of microtubules has been characterized to 3 nm resolution employing time-resolved X-ray scattering. This has revealed detailed structural features of microtubules not observed before in solution. The polymerization of highly purified tubulin, induced by the antitumour drug taxol, has been employed as a microtubule model system. This assembly reaction requires Mg^{2+}, is optimal at a 1:1 taxol to tubulin heterodimer molar ratio, proceeds with GTP or GDP and is intrinsically reversible.

The X-ray scattering profiles are consistent with identical non-globular α and β-tubulin monomers ordered within the known helical surface lattice of microtubules. Purified tubulin–taxol microtubules have a smaller mean diameter (approx. 22 nm) than those induced by microtubule associated proteins or glycerol (approx. 24 nm), but nearly identical wall substructure to the resolution of the measurements. This is because the majority of the former consist of only 12 protofilaments instead of the typical 13 protofilaments, as confirmed by electron microscopy of thin-sectioned, negatively stained and ice-embedded taxol microtubules. It may be concluded that taxol induces a slight reduction of the lateral contact curvature between tubulin monomers.

The main fringe pattern observed in cryo-electron micrographs is consistent with a simple 12 protofilament 3-start skewed lattice model. Cylindrical closure of this lattice can be achieved by tilting the lattice 0·8° with respect to the microtubule axis. The closure implies a discontinuity in the type of lateral contacts between the tubulin monomers (regardless of whether these are of the -α-β- or the -α-α-/-β-β- type), which indicates that lateral contacts and the subunit specificity of taxol binding are, to a large degree, equivalent.

Keywords: tubulin; taxol; microtubules; synchrotron X-ray scattering; cryo-electron microscopy

1. Introduction

Microtubules are the main organizers of cellular architecture, organelle transport and membrane traffic in the eukaryotic cell cytoplasm (Darnell *et al.*, 1990). Typical microtubules are long hollow cylinders of approximately 25 nm diameter, comprising 13 longitudinal protofilaments (Tilney *et al.*, 1973), although microtubules with other protofilament numbers are known (Chalfie & Thompson, 1982). The arrangement of tubulin subunits forming the microtubule wall was established by three-dimensional reconstruction of electron microscopy images of flagellar microtubules (Amos & Klug, 1974) and tubulin sheets (for reviews, see Amos, 1979; Amos & Eagles, 1987). The surface lattice of microtubules consists of a 13 protofilament 3-start left-handed helix with 12 nm pitch. The basic axial repeat is 4 nm, corresponding to the axial centre-to-centre distance between tubulin monomers (M_r 50,000). The functional assembly units are tubulin heterodimers (M_r 100,000), which are believed to be aligned head-to-tail along the protofilaments, forming -$\alpha\beta$-$\alpha\beta$- contacts. From one heterodimer to the next, along the three-start helix,

0022-2836/92/130169-16 $03.00/0

© 1992 Academic Press Limited

there are either heterologous (-α-β- and -β-α-) or homologous (-α-α- and -β-β-) lateral interactions, corresponding to the flagellar microtubule lattices type A and B, respectively. The low-resolution structure of microtubules was further characterized by electron microscopy (Amos, 1979; Amos & Eagles, 1987) and X-ray diffraction by oriented microtubule gels (Mandelkow *et al.*, 1977; Beese *et al.*, 1987; Wais-Steider *et al.*, 1987). At present, the more detailed microtubule structural model is the 1·8 nm resolution X-ray diffraction model by Beese *et al.* (1987), in which each monomer appears to consist of three domains and the α and β-tubulin monomers are indistinguishable. Interestingly, each tubulin chain has been found to consist of three major types of limited proteolysis fragments; however, the monomer structural domains need not be sequential (de la Viña *et al.*, 1988; Arevalo *et al.*, 1990). Due to lack of crystals, the high-resolution structure of tubulin is unknown.

Time-resolved synchrotron X-ray scattering has been extensively employed to study microtubule assembly in solution (Mandelkow *et al.*, 1980; Bordas & Mandelkow, 1982; Bordas *et al.*, 1983; Mandelkow & Bordas, 1986; Spann *et al.*, 1987; Marx *et al.*, 1990). These investigations have provided important insights into the mechanisms of microtubule assembly; studies were limited, however, to approximately 8 nm resolution, determining the microtubule diameter and wall thickness, but not accessing the substructure of the polymer wall. Higher angle static X-ray scattering patterns of microtubules and rings, in which the expected maxima were scarcely visible, have been previously recorded on film, employing long exposure times to synchrotron radiation (Mandelkow *et al.*, 1983).

During cell division, microtubules are the main constituents of the mitotic spindle and the target of mitosis-arresting drugs (Taylor, 1965; for a review, see Hamel, 1992). The anti-tumour alkaloid taxol (Wani *et al.*, 1971; Rowinsky *et al.*, 1990) has the unique property of being able to induce microtubule assembly (Schiff *et al.*, 1979). Taxol-induced assembly proceeds by an as yet unknown mechanism, and is driven by the preferential binding of this ligand to microtubules over unassembled tubulin (Parness & Horowitz, 1981; Carlier & Pantaloni, 1983; Howard & Timasheff, 1988).

We have employed the taxol-induced assembly of tubulin as a microtubule model system. The resolution of previous X-ray scattering measurements of purified calf brain tubulin (Andreu *et al.*, 1989) has been extended to approximately 3 nm, thus revealing structural features of the microtubule wall in solution† (Andreu *et al.*, 1991). These are very similar in taxol, glycerol and MAP‡-induced microtubules, and compatible with the main X-ray reflections in diffraction diagrams from oriented microtubules. The solution X-ray results have been complemented by electron microscopy of negatively stained, of thin sectioned and of frozen-hydrated microtubules. The majority of the taxol microtubules assembled from purified tubulin have the characteristic 3-start microtubule lattice, but with only 12 protofilaments.

† A preliminary report was presented at the meeting, The living cell in four dimensions, C.N.R.S., Gif-sur-Yvette, September 1990.

‡ Abbreviations used: MAP, microtubule associated protein; Ig, immunoglobulin.

2. Materials and Methods

(a) *Proteins and chemicals*

Tubulin was purified from calf brain, stored in liquid nitrogen and prepared for use as described elsewhere (Weisenberg *et al.*, 1968; Lee *et al.*, 1973; Andreu *et al.*, 1989). The protein was equilibrated in 10 mM-sodium phosphate buffer (pH 7·0) and 1 mM-GDP or GTP (Boehringer), 6 mM-$MgCl_2$ was added immediately after equilibration (final pH 6·7); taxol was added in the cold before assembly. This procedure gave results indistinguishable from those of direct equilibration in the complete buffer containing nucleotide and Mg^{2+}; however, it allowed partial nucleotide substitution in portions of the same initial solution (Howard & Timasheff, 1986) and gave better protein yields. Alternatively, tubulin was equilibrated in 10 mM-sodium phosphate, 3·4 M-glycerol (Merck), 1 mM-EGTA, 6 mM-$MgCl_2$, 1 mM-GTP (pH 6·5). Bovine brain microtubule protein (tubulin plus MAPs) was prepared by 3 cycles of assembly and disassembly without glycerol (Asnes & Wilson, 1979), stored in liquid nitrogen, and equilibrated by Sephadex G25 chromatography in 100 mM-Mes (Sigma), 1 mM-EGTA, 1 mM-$MgSO_4$, 1 mM-GTP (pH 6·8) before use. Microtubule assembly was routinely characterized by turbidity and electron microscopy (Andreu & Timasheff, 1986). Taxol was kindly provided by the National Cancer Institute, National Institutes of Health (Bethesda, MD), was dissolved in dimethylsulfoxide (Merck), stored at −20°C, and its concentration measured spectrophotometrically (Wani *et al.*, 1971). Residual solvent in the experiments was usually less than 1%, included also in controls.

(b) *X-ray scattering measurements*

The X-ray scattering experiments were performed at station 2.1 of the Daresbury Laboratory Synchrotron Radiation Source. The equipment and data reduction procedures have been described elsewhere (Bordas, 1989; Towns-Andrews *et al.*, 1989; Bordas *et al.*, 1983). The camera was set to cover ranges of scattering vectors **S** (defined as reciprocal Bragg spacings, i.e. $2(\sin\theta)/\lambda$) from approx. 0·01 nm^{-1} to approx. 0·33 nm^{-1}. The absolute values of the scattering vector were obtained by reference to the orders of the 67 nm repeat in wet rat tail collagen. The X-ray scattering profiles of tubulin solutions were recorded in 5 or 10 s time frames. Assembly was started by a temperature jump from 2°C to 37°C, measured by a thermocouple placed into the solution. Radiation damage due to the intense X-ray beam was avoided by employing a scanning sample cell (Andreu *et al.*, 1989). Upon rescanning the cell, tubulin remained functional and dimer and microtubule scattering patterns were identical to those obtained in 1st scans. Other control measurements performed on the monoclonal antibody C.AL 20-5 (a mouse anti-*p*-azophenyl arsonate $IgG_1(k)$: Slaughter *et al.*, 1982)

were satisfactory, indicating that this procedure may be useful for other proteins very sensitive to X-rays, such as the IgG molecules (Gregory *et al.*, 1987).

(c) *Interpretation of the X-ray solution scattering patterns*

The origin of the features in the low-resolution X-ray solution scattering of microtubules can be established by reference to their fibre diffraction diagrams, interpreted by helical diffraction theory (Klug *et al.*, 1958; Vibert, 1987) and indexed on the basis of the well-known surface lattice of microtubules (Amos & Klug, 1974). Assuming that the α and β subunits are identical, in our resolution range, the selection rule for the helical structure of microtubules is given by:

$$3l = n + 13m, \quad (1)$$

where l, n and m are integers defining, respectively, the layer line index, the helix multiplicity or Bessel function order contributing to the layer line and some integer number. A Bessel function of order n on any given layer will have its 1st maximum at approx. a reciprocal radial spacing given by:

$$R = (n+1)/\pi D, \quad (2)$$

where D is the diameter of the helix, except for $n = 0$ (i.e. a J_0 Bessel term) where the 1st maximum is on the origin. It follows from the selection rule and the diameter of microtubules that, in our resolution range, the equator ($l = 0$) will contain J_0 and J_{13} Bessel function contributions, and the 1st layer line ($l = 1$) will contain 2 pairs of J_3 and J_{10} Bessel maxima. For a 12 protofilament microtubule surface lattice the indexing is different, and the selection rule becomes:

$$3l = n + 12m. \quad (3)$$

In the case of the solution scattering patterns of randomly oriented microtubule samples, the intensity of each reflection is redistributed around a circle centred at the origin of the diffraction diagram (see Fig. 3, Mandelkow & Bordas, 1986). Multiplication of the solution scattering intensities by the modulus of the scattering vector, **S**, retrieves the intensities in the fibre diffraction diagram, but the relative orientation of the various maxima is lost. In our resolution range, the main Bessel maxima occur at different values of **S** and their intensities do not superimpose. Given the knowledge of the spacing between layer lines, the reciprocal radial positions of these maxima are obtained by simple triangulation.

(d) *Model calculations*

The tubulin monomer was represented by a group of closely packed spheres of 1·5 nm diameter. The best shape was selected by an iterative fitting algorithm based on Debye's formula (Guinier & Fournet, 1955), in which the solution scattering patterns of tubulin heterodimers were fitted (to be reported elsewhere). This monomer was then placed in a microtubule helical lattice of either 12, 13 or 14 protofilaments and the scattering profile was calculated employing the X-ray solution scattering simulation program DALAI (E. Pantos, D. Holden, J. West & J. Bordas, unpublished results) optimized for structures with helical symmetry. The monomer orientation was varied and its shape further optimized until the difference between the calculated and the measured microtubule pattern was minimized. Although the final fits are excellent (see Fig. 5) it must be stressed that there is no guarantee that the minimum between the calculated and the measured scattering patterns is either unique or the best one. These calculations serve the purpose of excluding unlikely monomer shapes and protofilament numbers.

(e) *Electron microscopy*

Microtubule solutions (non-fixed) were briefly adsorbed onto carbon-coated grids, negatively stained with 2% uranyl acetate and observed under a Philips EM 300 electron microscope. To obtain tannic acid-stained microtubule cross-section images (Tilney *et al.*, 1973), previously unassembled microtubule solutions were centrifuged at 356,000 *g* and 2°C in a pre-cooled TL100.2 rotor in the Beckmann TL100 ultracentrifuge for 3 h (by which time microtubule pellets had already formed due to the high local protein concentration). This was followed by a further 1 h spin with the temperature control set at 37°C. The pellets were processed as described elsewhere (Gil, 1988), with some modifications: they were fixed for 1 h with a freshly prepared mixture of 2% glutaraldehyde and 4% tannic acid, then postfixed with 4% osmium-tetraoxide, dehydrated, embedded in Epon, thin-sectioned to approximately 30 nm with a diamond knife in an LKB Ultramicrotome III and stained with uranyl acetate and lead citrate. Micrographs of the sections were obtained using Philips 300 and 301 electron microscopes. Cryo-electron micrographs (Taylor & Glaeser, 1976; Dubochet *et al.*, 1987) of non-fixed microtubules were obtained with a Philips 400 electron microscope equipped with a Gatan cryotransfer and anticontaminator. Specimen preparation and observation were essentially as described by Wade *et al.* (1989).

(f) *Interpretation of electron microscopy microtubule images*

The characteristic fringe patterns that are observed in lateral projections of well-preserved microtubules are the result of the superposition of the images of the protofilaments in the front and back microtubule walls (Mandelkow *et al.*, 1986). Analysis of these patterns allows us to characterize the number of protofilaments and the pitch of the helical microtubule surface lattice. Simulated microtubule mass projections for microtubules of different protofilament numbers and 2, 3 and 4-start lattices were generated using the program LEGO, and the type of pattern, repeat period and diameter of the observed microtubules were directly compared with them (Pantos *et al.*, 1988; Wade *et al.*, 1991).

3. Results

(a) *Taxol-induced assembly of purified calf brain tubulin into microtubules is stoichiometric and Mg^{2+}-dependent*

Figure 1 shows the time-resolved X-ray scattering profiles of a solution of tubulin and taxol whilst assembling in 10 mM-sodium phosphate, 6 mM-$MgCl_2$, 1 mM-GTP (pH 7·0) buffer. The initial frames were recorded at 2°C and are featureless, indicating the absence of ordered assemblies in the solution. However, the average radius of gyration of tubulin in this state was considerably larger (5·7 nm) than that of tubulin heterodimer (3·1 nm: Andreu *et al.*, 1989), indicating Mg^{2+}-induced tubulin oligomerization in the cold. After a temperature jump to 37°C, an increase in the

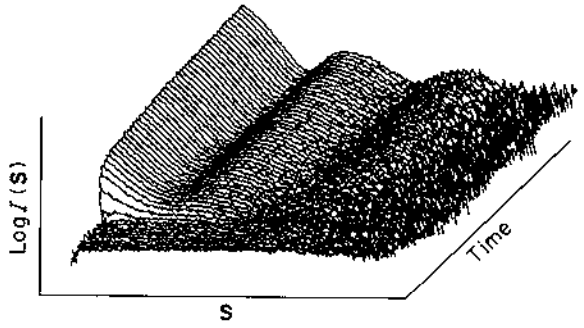

Figure 1. Time-resolved X-ray scattering of a 55 μM-tubulin–taxol solution during assembly (10 mM-sodium phosphate, 6 mM-$MgCl_2$, 1 mM-GTP, pH 7·0). The data were collected in 10 s time frames. The sample was loaded in the cold and the temperature was increased from 2 °C to 37 °C at frame 10.

central scattering, due to the increase of the overall degree of polymerization, was observed. Also, the appearance of the maxima corresponding to the J_0 Bessel function, corresponding to the low resolution transform of the hollow cylindrical structures, was detected. Samples did not show any long-range orientation effect. Cooling the samples to 2 °C resulted in partial disassembly. At sufficiently low protein and Mg^{2+} concentrations (below 20 to 30 μM and 4 to 6 mM, respectively), disassembly was noticeable in the X-ray scattering profiles after approximately two hours. When monitored by light scattering (not shown), disassembly appeared complete. Both observations clearly indicate reversibility. In contrast, higher protein or Mg^{2+} concentrations resulted in the formation of cold-stable microtubules, and also in slow polymerization in the cold. Similarly, taxol assembly proceeded at approximately 10 °C. This study focuses on the structure of the purified tubulin–taxol microtubules under optimal assembly conditions. The assembly process was examined as a function of taxol, Mg^{2+} and protein concentrations. Figure 2 shows the X-ray scattering profiles of solutions of 30 μM-tubulin and varying taxol concentrations at 37 °C. Microtubule assembly did not proceed without taxol or Mg^{2+} (Fig. 2(a), continuous and broken lines, respectively), though the Mg^{2+}-induced tubulin oligomerization was detected by the increase in central scattering. The polymerization was maximal at a stoichiometric 1 : 1 taxol to tubulin molar ratio (Fig. 2(d)). At larger taxol to tubulin ratios (see profiles (e) and (f) in the Fig.) the overall degree of polymerization remained sensibly invariant; however, the microtubule features (the intensities of the 1st, 2nd and 3rd maxima of the J_0 Bessel function relative to the absolute scattering intensity) were less defined. Optimal Mg^{2+} concentrations were between 6 mM and 16 mM. The effects of pH were apparently weak between pH 6·5 and 7·0. In view of the above results, the experiments throughout the rest of this study were performed at essentially 1 : 1 taxol to tubulin molar ratio in 6 mM-

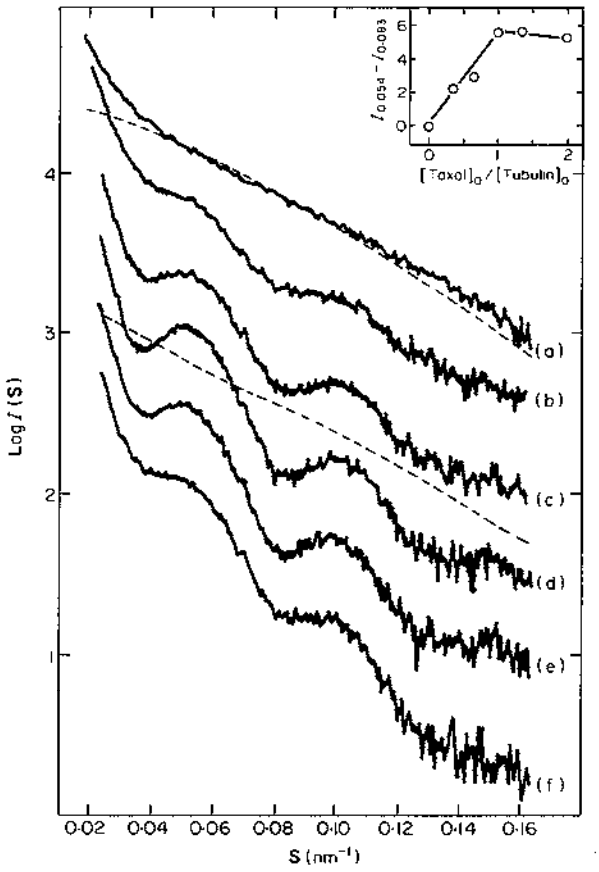

Figure 2. Stoichiometry of taxol-induced microtubule assembly. Final assembly states of 30 μM-tubulin equilibrated in 10 mM-sodium phosphate, 6 mM-$MgCl_2$, 1 mM-GTP, pH 6·5. (a) No taxol (broken line, no $MgCl_2$ with taxol); (b) 10 μM-taxol; (c) 20 μM-taxol; (d) 30 μM-taxol (broken line, initial state in the cold); (e) 40 μM-taxol; (f) 60 μM-taxol. Inset: peak to valley intensity (arbitrary units) of the 1st J_0 subsidiary maximum as a function of the taxol to tubulin mole ratio.

Mg^{2+} (pH 6·7) buffer. Varying the tubulin–taxol concentration indicated that the critical concentration for assembly was well below the practical sensitivity of the X-ray instrument (approx. 10 μM-tubulin). Above 60 μM-tubulin–taxol the profiles obtained could be ascribed, by comparison with model mixture profiles (Bordas *et al.*, 1983), to mixtures of more than 95% microtubules with less than 5% unassembled tubulin.

(b) *Solution X-ray scattering profiles of microtubules to 3 nm resolution. Smaller diameter and same surface lattice of taxol microtubules compared with glycerol and MAP-induced microtubules*

Figure 3(a) displays the scattering patterns of microtubules assembled from purified tubulin–taxol in GDP buffer (profile (1)) and in GTP buffer (profile (2)). As drug-free controls, microtubules were also assembled from microtubule protein (tubulin plus assembly-inducing MAPS; profile (3)) and purified tubulin in glycerol buffer (profile (4)).

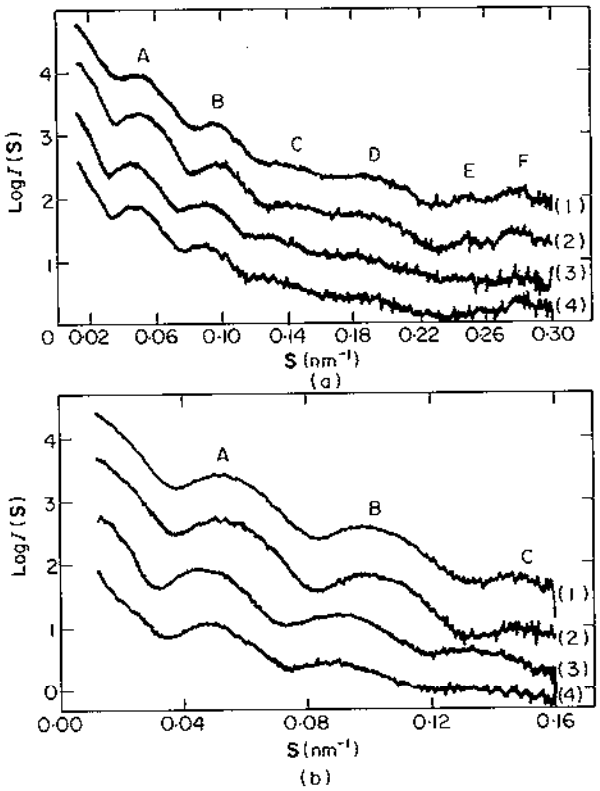

Figure 3. (a) X-ray scattering profiles of microtubules of different composition (buffers and sample preparation are described in Materials and Methods). The profiles were recorded with a 3 m camera; they are displaced in the ordinate axis to facilitate comparison. (1) 200 μM-tubulin–taxol, 1 mM-GDP; (2) 200 μM-tubulin–taxol, 1 mM-GTP; (3) 7·8 mg ml^{-1} microtubule protein; (4) 48 μM-tubulin in glycerol buffer. (b) Experiments equivalent to (a) but profiles measured with a 6 m camera.

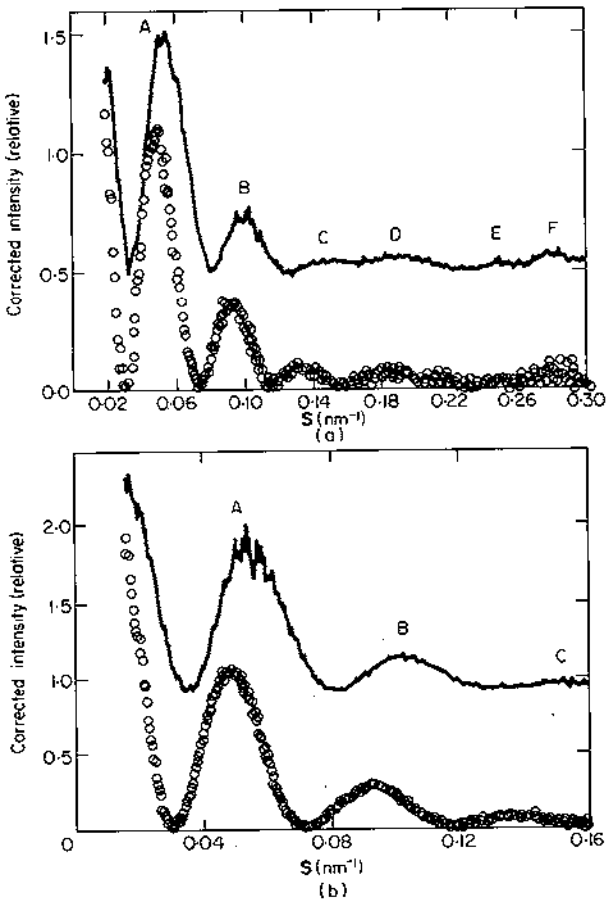

Figure 4. X-ray scattering corrected intensity profiles of microtubules made of purified tubulin–taxol (continuous trace) and of microtubule protein (circles). These profiles have been obtained by multiplying the scattering intensities (same data as Fig. 3) by their corresponding **S**-axis and subtracting a polynomial passing through the expected zeros, i.e. the positions in which the circularly integrated intensities of microtubule diffractograms are null.

Glycerol is a non-specific thermodynamic enhancer of tubulin polymerization (Lee & Timasheff, 1975; Na & Timasheff, 1981*a*). Figure 3(b) shows the equivalent scattering patterns obtained with a longer camera length, for which the low angle region is better defined. The profiles of taxol microtubules with GDP and GTP are nearly identical, though the peak intensities are slightly larger in GTP. The glycerol and the MAP-containing microtubule profiles are similar, except for the minimum between maxima D and E, which is clearly less marked in microtubule protein. The profiles of taxol and control microtubules are similar at high angle (maxima D, E and F), whereas a marked displacement of the maxima A, B and C to larger scattering vector values is observed.

Figure 4 shows the corrected scattering intensities of taxol and microtubule protein microtubules. These profiles have been obtained by multiplying the X-ray scattering intensities by their corresponding **S**-axis and subtracting the analytically estimated incoherent scattering from the patterns. This procedure corrects the solution scattering intensities for the radial dilution effect caused by the random orientation of microtubules in solution (Materials and Methods). Better definition of the position of the maxima and a more direct comparison of solution scattering to fibre diffraction patterns is facilitated using this approach.

The position and indexing of the X-ray scattering maxima of taxol and control microtubules are given in Table 1. The peaks A, B and C are the first, second and third subsidiary maxima of the equatorial J_0 Bessel function, which are sensitive to the diameter and wall thickness of the microtubules (see Materials and Methods). The average ratio of their positions in taxol to control microtubules is $1{\cdot}09 \pm 0{\cdot}01$, indicating that the mean diameter of taxol microtubules is only $91{\cdot}7(\pm 0{\cdot}9)\%$ that of control microtubules. The scattering bands D, E and F originate from the surface lattice of microtubules. Their relative intensities and, to a much lesser extent, their positions are dependent on the monomer structure (see Materials and Methods). The scattering band D corresponds to the equatorial

Table 1

Characteristics of the X-ray scattering profiles of microtubules of different composition

Type of microtubules	Scattering maxima and position S (nm^{-1}) A	B	C	D	E	F	Mean helical radius† (nm)
Purified tubulin–taxol‡	0·0538 (J_0)	0·100 (J_0)	0·150 (J_0)	0·192 (J_{12})	0·253 (J_3)	0·281 (J_9)	10·8 (11·2)
Microtubule protein	0·0500 (J_0)	0·092 (J_0)	0·134 (J_0)	0·192 (J_{13})	0·250 (J_3)	0·282 (J_{10})	12·0 (12·1)
Purified tubulin–glycerol	0·0496 (J_0)	0·092 (J_0)	0·137 (J_0)	0·190 (J_{13})	0·25 (J_3)	0·281 (J_{10})	12·0 (12·2)
Microtubule protein–taxol	0·050	0·095	0·142	0·19	0·25	0·28	11·8 (12·0)
Purified tubulin–glycerol–taxol	0·053	0·102	0·15	0·19	0·25	0·28	10·8 (11·2)

† Radii measured by application of model-fitting simple tubular structures (Bordas *et al.*, 1983). Numbers in parentheses are helical radii estimated from the positions of the 1st and 2nd subsidiary maxima of the J_0 Bessel function (Abramowitz & Stegun, 1965).

‡ The position of the maxima for microtubules assembled in GTP and GDP coincided within experimental error (approx. $\pm 0{\cdot}001\ nm^{-1}$).

J_n Bessel function and gives the mean lateral interprotofilament spacing. This is identical for taxol and MAP-induced microtubules. Whilst the reciprocal of the **S** value gives a spacing of 5·2 nm, the result obtained from modelling of the scattering profile (see Fig. 5) is 5·7 nm; this is because the grooves between the protofilaments are displaced to the outside of the microtubule, i.e. the inside is flatter. The scattering bands E and F result from the maxima in the first layer line. These arise from electron density features in the direction of the helices defined by the microtubule wall lattice (i.e. the 3-start and 10-start helices in 13 protofilament microtubules). Their positions are identical in taxol and control microtubules; the simplest interpretation is that the axial intermonomer spacing and periodic helical features are the same in both types of microtubules. With the assumption that the tubulin subunits in taxol and control microtubules are similar, the coincidence of the positions of bands D, E and F indicates that the wall lattice is, within the resolution of the measurements, the same for both types of microtubules. It follows then, that in order for taxol microtubules to have a smaller diameter, they must have on average approximately one protofilament less than the control microtubules. An alternative explanation would be that taxol microtubules had the same number of protofilaments, but closer together. However, their lateral interprotofilament spacing would be smaller and band D would occur at approximately $0{\cdot}210\ nm^{-1}$, which is well outside experimental error in the position of the maxima and cannot be the case†.

When purified tubulin was assembled with both glycerol and taxol, a displacement of the J_0 maxima to positions close to the purified tubulin–taxol microtubules was observed. However, assembling microtubule protein in the presence of taxol had a much weaker effect (Table 1).

(c) *Modelling purified tubulin–taxol microtubules to 3 nm resolution is only compatible with 12 protofilaments and defines a possible tubulin monomer shape and orientation*

Having characterized the low resolution structure of taxol microtubules by comparison with microtubules assembled without taxol, we sought to define the structure of taxol microtubules by direct computer model-fitting of their solution scattering intensity profiles. Initially, calculations were carried out using a 13 protofilament 3-start helical surface lattice (Amos & Klug, 1974), subsequent models were calculated allowing the number of monomers per turn to vary. The monomers were modelled first using single spheres, for which only 12 protofila-

† Notice that the smaller diameter of taxol microtubules compensates for the different Bessel function indexing (Table 1). By the same reasoning, the interpretation above is valid regardless of the fact that these microtubules are a mixed population of different protofilament numbers (see electron microscopy results). It could be argued that taxol microtubules may have predominantly 13 protofilaments, with band D remaining at the same position because the grooves on the outside of the microtubule partially close and are displaced to a larger mean diameter by the protofilaments coming close together. However, this would have 2 effects. 1st, the intensity of band D would be smaller (less contrast) in taxol microtubules, which is not observed. 2nd, such laterally compressed lattice would have the monomers closer also in the 3-start and 10-start directions, resulting in a displacement of bands E and F to larger scattering vector values; however, these maxima remain at identical positions. It could then be argued that the electron density features giving rise to these bands are displaced to such larger diameters that leave these maxima in identical positions in the compressed lattice. However, this is very unlikely and, again, the expected intensities of bands E and F would be smaller in the taxol than in the non-taxol microtubules, which is contrary to experience.

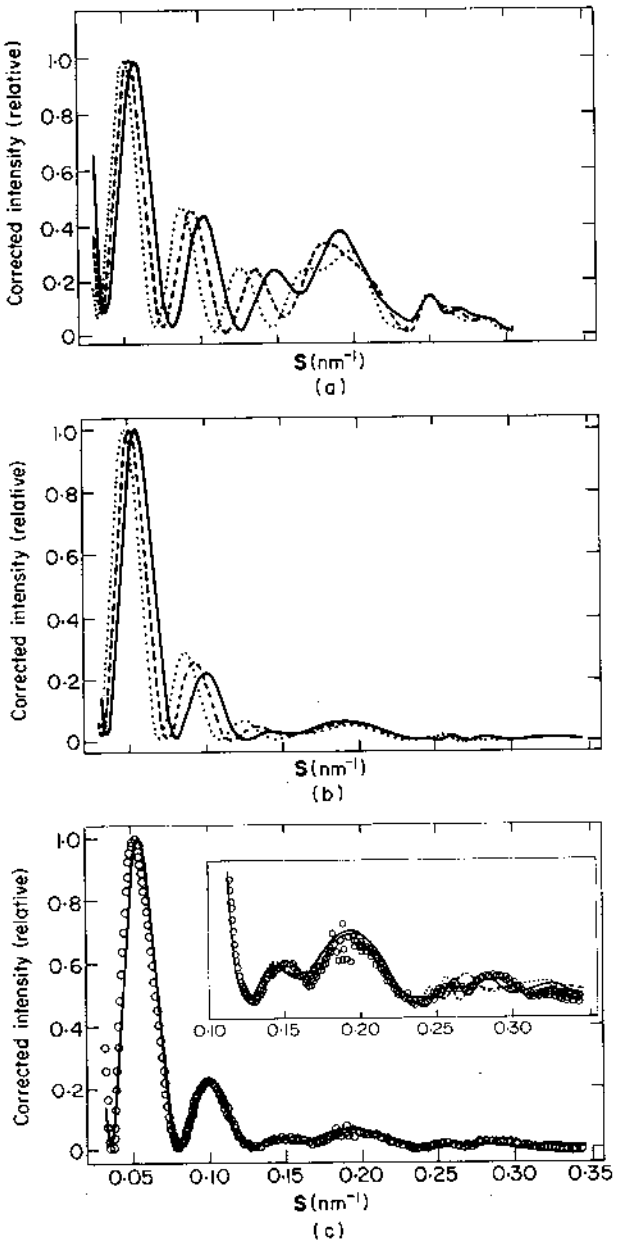

Figure 5. (a) Model calculations of the X-ray scattering profiles for 12 (continuous line), 13 (broken line) and 14 protofilament (dotted line) microtubules in which the tubulin monomer has been approximated by a sphere of diameter approx. 7 nm. (b) As above, but the tubulin monomer has been approximated by a series of spheres of diameter 1·5 nm, with a morphology deduced to provide the best fit to the experimental data. (c) Best fitting 12 protofilament microtubule model (continuous line) and experimental data (circles); the inset is an enlargement of ordinate scale showing the 2-start (dotted line), 3-start (continuous line) and 4-start lattice (broken line) models.

ment microtubules fitted the positions of the lower angle maxima. The fit of the intensities at higher angle, as shown by Figure 5(a), was poor. In order to fit the higher angle scattering features it was necessary to depart significantly from globular monomer models. Figure 5(b) shows the scattering profiles of such 12, 13 and 14 protofilament microtubule models (see Materials and Methods, section (d)). Of all the models examined, only those with 12 protofilaments fitted the data at low angle, whilst the 13 and 14 protofilament models did not. Figure 5(c) compares the best model (continuous line) with the data (circles). To approach the experimental scattering profile at higher angle, the monomers were oriented with their major axis pointing towards the microtubular centre, and a secondary axis oblique to the protofilament axis. However, the possibility still exists for these microtubules to have different surface lattices. Changing from a 3-start to 2-start or to a 4-start helical lattice produced very similar model scattering profiles at low angles. Some differences can be observed in the region above 0·25 nm^{-1} (see inset in Fig. 5(c)), but they are not sufficient to be unequivocally distinguished by the solution scattering data.

(d) *Electron microscopy of the purified tubulin–taxol assembly products: majority of 12 protofilament 3-start microtubules*

In order to test the structure of taxol microtubules derived from the X-ray results by independent procedures, they were observed in ultrathin sections, in negatively stained preparations and by cryo-electron microscopy. The majority of taxol microtubule cross-sections stained by the tannic acid procedure corresponded to 12 protofilaments, though microtubules made of 13 and other protofilament numbers were also observed, along with opened tubular structures and microtubule pairs (see Fig. 6).

Figure 7(a) is a representative electron micrograph of a negatively stained taxol microtubule and Figure 7(b) is a glycerol microtubule. The difference in diameter is apparent. The glycerol microtubule image essentially shows two continuous longitudinal fringes, slightly off-centre, corresponding to a 13 protofilament 3-start lattice model. The majority of taxol microtubules show the characteristic pattern of two fringes-blur-one fringe-blur of Figure 7(a). The pattern and estimated repeat period (355($\pm$44) nm) correspond to a 12 protofilament 3-start lattice and deviate significantly from 2-start and 4-start models.

Since negatively stained specimens may be distorted by flattening during drying (though the taxol microtubules seem more resistant) or by the stain, unstained ice-embedded microtubules were also examined. Figure 8(e) is a representative field of view of purified tubulin–taxol microtubules. The majority (approx. 60%) of the taxol microtubules examined by cryo-electron microscopy showed the two fringe-one fringe pattern (period approx. 300 nm), and had a diameter of approximately 22 nm, only compatible with the 12 protofilament 3-start lattice. A smaller number of images (approx. 40%) corresponded to the 13 protofilament 3-start lattice, with diameter approximately 23 nm. Figure 8(b) is a cryo-electron micrograph of microtubules assembled from microtubule protein, which shows

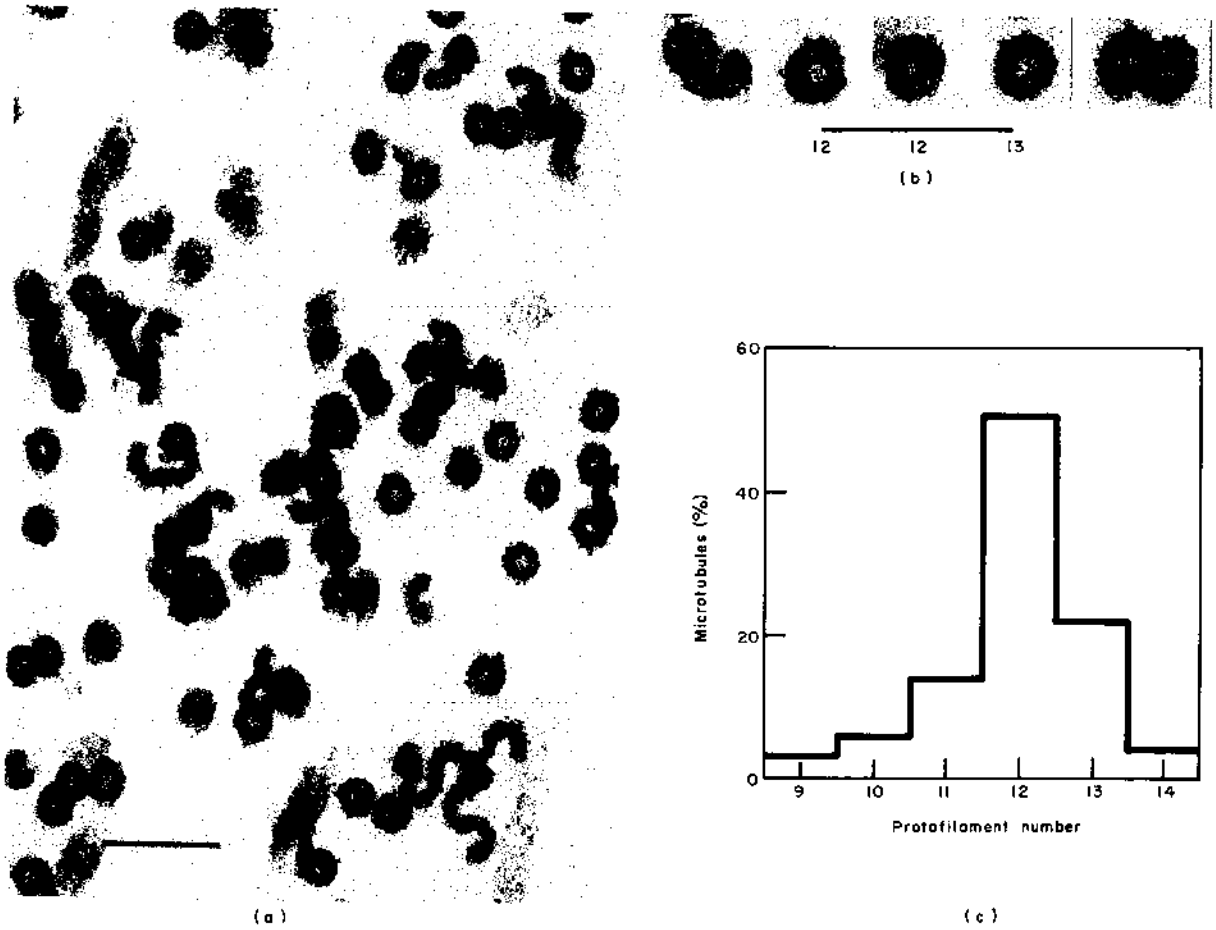

Figure 6. Electron micrograph of a tannic acid stained thin sectioned tubulin–taxol microtubule pellet. (b) Characteristic microtubule transverse sections observed, with the number of protofilaments indicated; the bars represent 100 nm. (c) Distribution of protofilament numbers.

mainly the three fringes-blur-two fringes-blur pattern with an approximate period of 500 nm and an approximate diameter of 24 nm. This is characteristic of a 14 protofilament 3-start model. Approximately 70% of the microtubule protein microtubules observed were of this type and 30% were of the 13 protofilament 3-start type with diameter approximately 23 nm. Note that from these results the average numbers of protofilaments would be approximately 12·4 and 13·7 in the taxol and microtubule protein preparations, respectively. The ratio of these values (0·905) is compatible with the diameter ratio measured using X-rays (0·91 ± 0·01). The cryo-electron micrographs and image interpretation of the non-taxol microtubules are in agreement with those of Wade *et al.* (1990); a single 12 protofilament 3-start microtubule image was reported (Chrétien *et al.*, 1990), which is similar to the tubulin–taxol microtubules.

Figure 9(a) and (b) compare a single ice-embedded taxol microtubule and the mass projection of a 12 protofilament 3-start microtubule model, respectively. In order to produce a fringe pattern of the type observed (period approximately 300 nm), it is necessary to azimuthally rotate each axially consecutive monomer in the 12 protofilament microtubule by about 0·4° relative to its position in an untwisted 13 protofilament lattice; this is independent of the twisting mechanism.

4. Discussion

(a) *Taxol-induced assembly of purified tubulin: a model system for microtubule assembly*

The tubulin used in these experiments is a highly purified and extensively characterized protein preparation (Na & Timasheff, 1981*b*; Lee, 1982; Andreu *et al.*, 1989) which, together with taxol, constitutes a rigorously defined model system for the study of microtubule assembly. This simplified system dispenses with the requirements of MAPs for the assembly of tubulin into microtubules, and also offers significant advantages over the assembly induced by cosolvents such as glycerol (Lee & Timasheff, 1975; Na & Timasheff, 1981*a*; Fig. 3 in this study). These advantages are the larger extent of assembly, the good stability of the assembled protein and the greater contrast for X-ray scattering studies. Temperature dependent reversible assembly of taxol treated microtubules can be obtained with millimolar Ca^{2+} concentrations (Collins & Vallee, 1987), whilst moderately alkaline

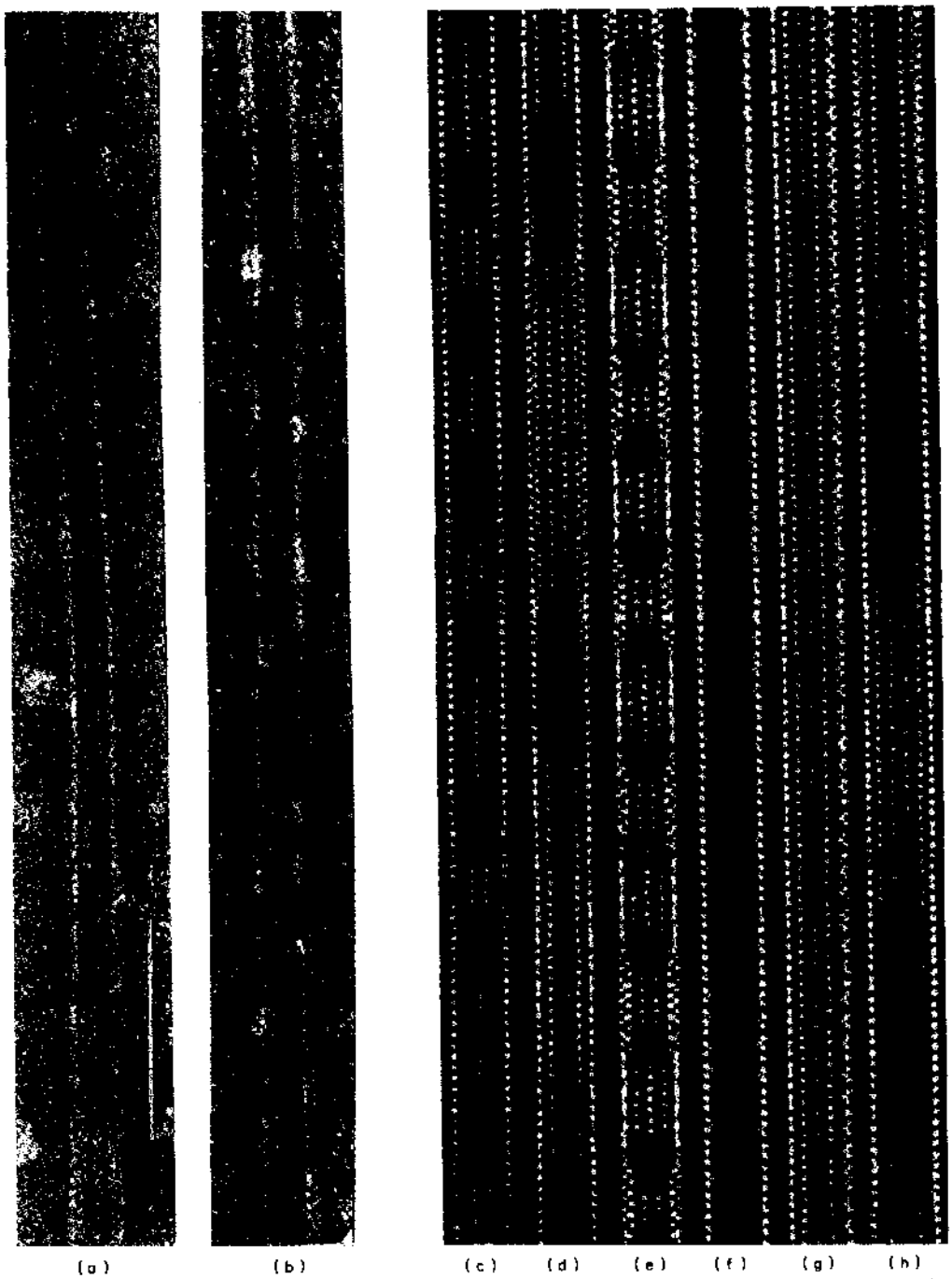

Figure 7. (a) Electron micrograph of a negatively stained purified tubulin–taxol microtubule. (b) A single microtubule assembled from purified tubulin in glycerol buffer. The bar represents 100 nm. The rest of the Fig. ((c) to (h)) shows model mass projections, obtained from a variety of microtubule lattices, showing characteristic fringe patterns. (c) 12 protofilaments, 2-start helix; (d) 12 protofilaments, 3-start helix; (e) 12 protofilaments, 4-start helix; (f) 13 protofilaments, 3-start helix, paraxial microtubule projected with back and front central protofilaments staggered; (g) same as (f) but projected with back and front central protofilaments superimposed; (h) 14 protofilament, 3-start helix. The repeats in the fringe patterns are 123·5, 411·5, 77·3, 0, 0 and 480·1 nm, respectively. The inter-protofilament separation in these models is 5·85 nm, which corresponds to the spacing in a 13 protofilament microtubule with a diameter of 24·2 nm. The monomers have been approximated with single spheres of 2·0 nm radius. All of the 12 protofilament models yield a pattern consisting of fringe-blur, two fringes-blur sequence. However, only the 3-start helical lattice (d) yields a fringe period compatible with the observation of a negatively stained purified tubulin–taxol microtubule (a). The microtubule (b) corresponds to the 13 protofilaments model (g).

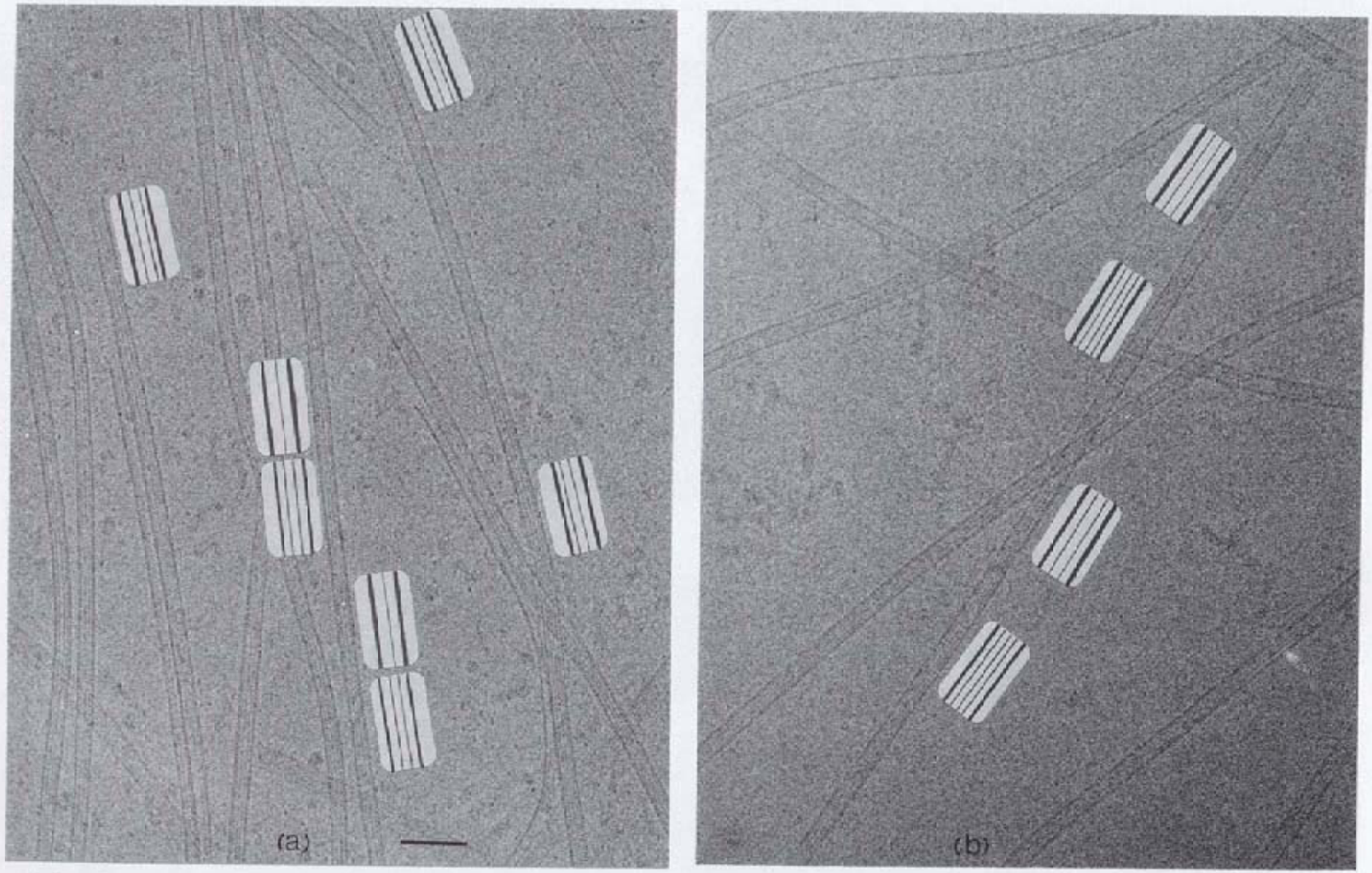

Figure 8. Cryo-electron micrographs of microtubules assembled from (a) purified tubulin–taxol or (b) from microtubule protein. Examples of the different fringe patterns observed in these fields are indicated. Bar represents 100 nm.

pH weakens the polymerization and allows the reversible disassembly of taxol microtubules (Ringel & Horwitz, 1991). In this study we have described conditions for the cold disassembly of purified tubulin–taxol microtubules, simply involving reduction of Mg^{2+} and tubulin concentrations. It must be concluded that the tubulin–taxol assembly is intrinsically reversible, although the critical concentration and the rate of polymer dissociation are strongly dependent on the experimental conditions.

Taxol induces the assembly of tubulin in both GTP and GDP buffer, in agreement with previous reports (Schiff & Horwitz, 1981; Howard & Timasheff, 1988; Carlier & Pantaloni, 1983; Williams & Rone, 1989), although the assembly kinetics are markedly different (unpublished results). The slow dissociation of taxol-induced microtubules and the effects of taxol on the assembly process, GTP hydrolysis and tubulin exchange (Carlier & Pantaloni, 1983; Wilson *et al.*, 1985), suggest that microtubule dynamic instability (Mitchinson & Kirchner, 1984) should be eliminated in taxol microtubules. Taxol-induced assembly should therefore be amenable to characterization in terms of a simple nucleated condensation polymerization process (Oosawa & Asakura, 1975). The fact that maximal polymerization was obtained at a 1 : 1 taxol to tubulin molar ratio is fully consistent with the binding of one taxol molecule per assembled tubulin heterodimer with high apparent affinity (Parness & Horwitz, 1981; Takoudju *et al.*, 1988*a*,*b*). However, the relative weakening of the microtubule features in the X-ray scattering patterns (Fig. 2) at over-stoichiometric taxol concentrations could be taken as an indication that additional taxol binding, to lower affinity sites, drives the assembly of tubulin into polymers other than closed microtubules.

(b) *Taxol induces the formation of microtubules with 12 protofilaments in which the tubulin monomers are arranged in a 3-start helix surface lattice: requirement of a discontinuity in the surface lattice*

The conclusion from the X-ray scattering observations is that the taxol microtubules have on average one fewer protofilament than the control microtubules, yet their surface lattice is approximately the same. If a major proportion of the microtubules assembled from microtubule protein had 13 protofilaments, the taxol microtubules would have 12 protofilaments. However, depending on the conditions of assembly, 13, 14 and 15 protofilament microtubules are known to be present in solutions of microtubule protein (Mandelkow *et al.*, 1986; Wade *et al.*, 1989). The model calculations verified that a major fraction of the taxol microtubules must have 12 protofilaments. The only condition imposed in the model calculations was that the taxol microtubules have the known, 3-start helix, surface lattice (Amos & Klug, 1974).

The taxol-induced reduction in microtubule diameter was observed in microtubules assembled from purified tubulin even in conditions not requiring taxol for assembly (i.e. glycerol buffer plus taxol, Table 1). This indicates that taxol, rather than the conditions of assembly, is the agent that decreases the number of protofilaments in microtubules assembled from purified tubulin. However, as shown by the weak effect of taxol on the diameter of the MAP containing microtubules (Table 1), microtubules assembled in the presence of taxol will not always have a reduced number of protofilaments. In many respects the action of taxol parallels that of MAPs, and the latter result suggests that taxol binding in the presence of MAPs does not result in the structural perturbation. However, it has been reported that taxol influences the control of protofilament number at microtubule-nucleating sites in *Drosophila* wing cultures, inducing a majority of 12-protofilament microtubules (Mogensen & Tucker, 1990).

The electron microscopy results confirmed and extended the X-ray scattering analysis. The majority of taxol microtubule images corresponded to the 12 protofilament 3-start lattice. In order to fit the lattice to one protofilament fewer, it is necessary to make incorrect cylinder closure contacts (i.e. out of register by -0.937 nm), or to uniformly increase the staggering of the monomers along the 3-start helix (by 0·078 nm), or to tilt the protofilament axis with respect to the cylinder axis. The latter does not require lattice distortion. Comparison of the taxol microtubule fringe pattern in the electron micrographs with model patterns suggests that the adjustment is made by the mechanism of lattice tilting. As shown in Figure 10, a small clockwise tilt, with respect to the cylinder axis (0·8°), of the protofilaments in the paraxial arrangement in the 13 protofilament microtubule is sufficient to produce the contacts leading to the 12 protofilament lattice. In this mechanism the resulting azimuthal rotation per monomer is $0{\cdot}31(\pm 0{\cdot}02)°$, which is close to the 0·4° value determined by model adjustment to the data (Fig. 9). Therefore, this is the simplest model that accounts for the results, although some lattice distortion cannot be ruled out. On the other hand, a certain deviation from paraxiality in the starting 13 protofilament microtubule cannot be excluded. Actually, the electron micrographs show that a deviation from side to side of the two longitudinal fringes, which is not compatible with a paraxial lattice, is noticeable in 13 protofilament taxol microtubules (see Fig. 8(a)), as well as in 13 protofilament glycerol (see Fig. 7(b)) and microtubule protein microtubules (not shown). Such effect could well justify the approximately 0·1° angle difference between the simple skewed lattice model and the observation in the taxol microtubules. A skewed lattice mechanism (with opposite angle) has been applied to explain microtubule lattice accommodation to more than 13 protofilaments (Langford, 1980; Wade *et al.*, 1990). The taxol-induced microtubules essentially confirm the computer model predictions for 12 protofilament microtubules (Fig. 7; Wade *et al.*, 1991).

A consequence of having only 12 protofilaments,

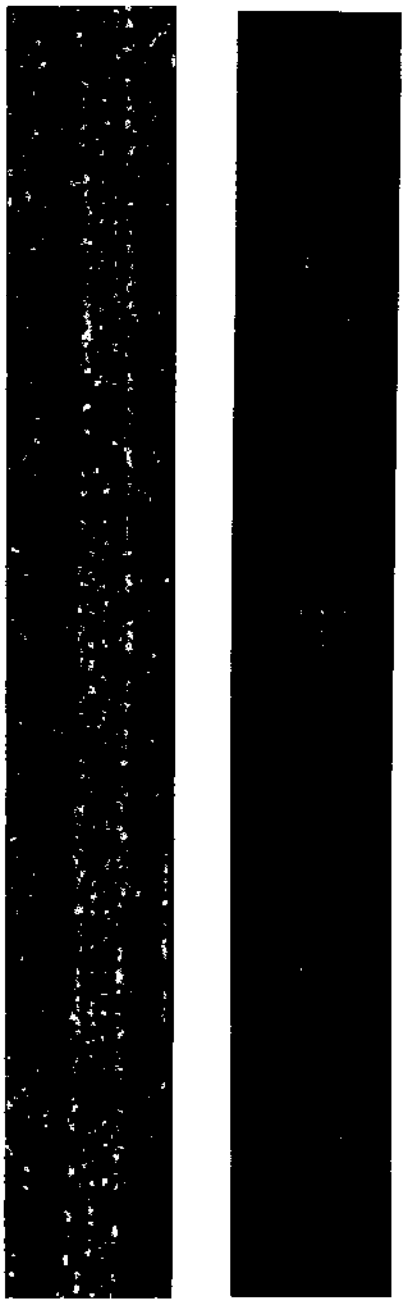

Figure 9. Cryo-electron micrograph of (a) a 12 protofilament microtubule assembled from purified tubulin and taxol and (b) a mass projection from 12 protofilament microtubule model showing the same fringe pattern. The model was constructed using the same monomer that fits the X-ray solution scattering pattern (Fig. 5) with 12·04 subunits/turn, mean diameter 21·8 nm and pitch 12·33 nm. The fringe repeat is 307·5 nm.

with the 3-start microtubule lattice, is that irrespective of choosing the type A or type B lattice (Amos & Klug, 1974), the closure between the first and 12th protofilaments belongs to the opposite lattice type. Hence, in these taxol microtubules there is necessarily a lattice-type change, or a propagated mixed lattice, which is made to close the cylinder (see Fig. 10). This implies that lateral bonds between the α or β subunits are equivalent to a large degree.

(c) *Low resolution structure of the tubulin monomer in taxol microtubules*

Modelling the X-ray scattering profile of tubulin–taxol microtubules, with spherical monomers of different radii, approximately fitted the positions of the centroids of the scattering bands, but did not reproduce their intensities. It was necessary to model the monomer shape and orientation. The resulting microtubule model (see Fig. 11) cannot be demonstrated to be unique; however, it describes the structure of the taxol microtubules in solution to 3 nm resolution. The model simply derives from interpreting the solution scattering pattern in terms of a 12 protofilament microtubule with the helical surface lattice described by Amos & Klug (1974), and adjusting the monomer to fit the profile, without any other assumptions. Some of the features of this model can be detected in the electron microscopy and X-ray fibre diffraction models (Amos & Klug, 1974; Mandelkow *et al.*, 1977; Beese *et al.*, 1987), although in the latter the resolution is higher than in our case and it shows additional features. At this stage, the modelling of the monomer from the solution data is tentative and its substructure is not well defined. Newly developed searching algorithms based on the Debye formula are being employed to simulate recently obtained X-ray solution scattering profiles of unassembled tubulin and taxol microtubules to 2 nm resolution.

(d) *X-ray solution scattering by microtubules compared with fibre diffraction*

Solution X-ray scattering profiles of microtubules from microtubule protein or purified tubulin in glycerol buffer were very similar. This supports the view that the structures are the same and that the MAPs are, by and large, flexible molecules that protrude from the microtubule wall (Vallee, 1980; Woody *et al.*, 1983; Hernandez *et al.*, 1986) and, consequently, do not contribute significantly to the features in the X-ray diffraction patterns from microtubules (Mandelkow, 1986; Beese *et al.*, 1987). The radial positions and corrected intensities of the solution scattering patterns are compared with available fibre diffraction data in Table 2. Small differences in the positions of the equatorial J_0 maxima are attributed to differences in mean diameter, as discussed above. The positions of the equatorial J_{13} reflections nearly coincide and the radial positions and intensity ratio of the two reflections measured in the first layer line are similar. This similarity, only barely observed previously (Mandelkow *et al.*, 1983), confirms the indexing based on the Amos & Klug (1974) lattice.

(e) *Mechanisms of induction of microtubule assembly by taxol*

In order to induce tubulin assembly by preferential binding to microtubules (Introduction), taxol

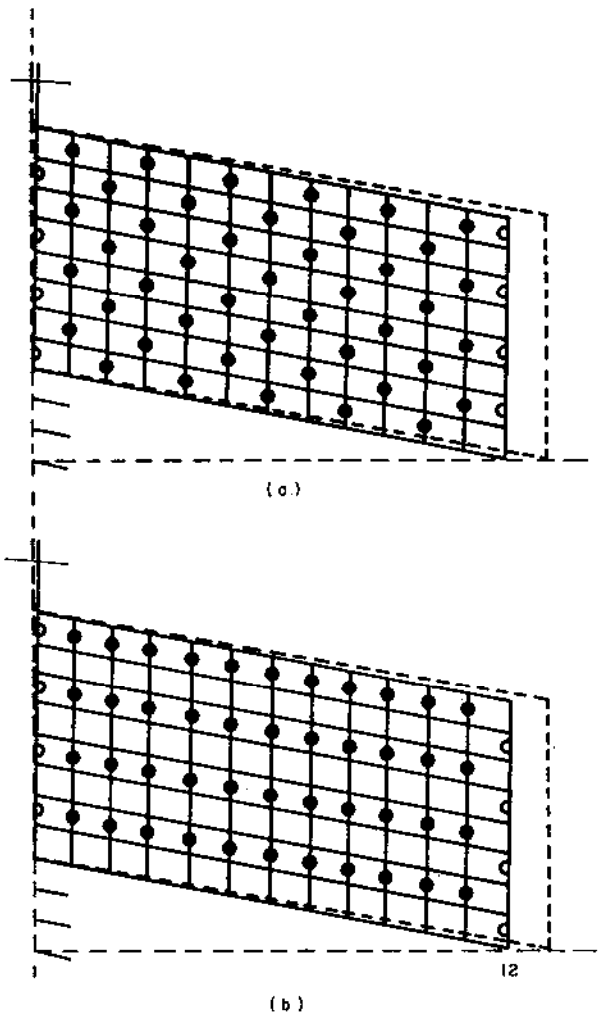

Figure 10. (a) Unrolled 12 protofilament 3-start microtubule lattice (continuous lines), obtained by taking out 1 protofilament from the known 13 protofilament lattice (broken lines) and tilting the lattice by a small angle with respect to the axis of the cylinder (shown unrolled). The filled circles indicate hypothetical taxol binding sites constituted by the lateral contact interface between tubulin molecules, considering a stoichiometry of 1 taxol molecule per heterodimer, and assuming subunit specificity (i.e. taxol binding to either the α/β or β/α lateral interfaces). The drawing corresponds to microtubule lattice type A. Notice that the subunit lattice necessarily presents a discontinuity caused by the cylindrical closure between protofilaments 1 and 12. Closure of the 12 protofilament microtubule implies a discontinuity also in the taxol lattice. This can be due to either a lack of taxol binding at the closure, a switching in the taxol to monomer binding specificity (as shown by the empty circles in the figure), or a mixed taxol lattice. In this model the taxol binding sites have been drawn between vicinal tubulin molecules, but this conclusion would be the same if they were assigned to one of the monomers. (b) Model equivalent to that shown in (a) but for lattice type B.

should increase contacts between tubulin molecules. Taxol induces a slightly larger curvature of the lateral bonds (i.e. an angle of 150° instead of 152·3°), resulting in taxol microtubules characteristically closing with 12 protofilaments. Two important questions are: what are the taxol binding sites within the microtubules? and how does this ligand-induced assembly proceed?

The comparative thermodynamic analysis of the effects of taxol on the polymerization of microtubules and the tubulin–colchicine polymer has led to the conclusion that taxol need not change qualitatively the mechanism of microtubule assembly, and to the suggestion that taxol would bind at the lateral interaction zones between tubulin molecules, thus bridging protofilaments (Howard & Timasheff, 1988). The Mg^{2+}-induced isodesmic self-association of GDP–tubulin, leading to double rings (Howard & Timasheff, 1986), appears not to be modified by taxol in the cold, as examined by sedimentation velocity and X-ray scattering (unpublished results). Since rings are considered structurally equivalent to coiled protofilaments (Mandelkow *et al.*, 1983), this suggests that taxol does not induce protofilament formation itself, but should induce the lateral association of different protofilaments, in favour of the model described by Howard & Timasheff (1988).

Table 2

Comparison of the positions of the X-ray diffraction maxima of microtubules in solution and in oriented fibres

Microtubule specimen	A (J_0)	B (J_0)	C (J_0)	D (J_{13})	E (J_3)	F (J_{10})
			R (nm^{-1})			
Solution†	0·050	0·092	0·134	0·192	0·045	0·138
	(1·00)	(0·24)	(0·03)	(0·07)	(0·01)	(0·02)
Fibre‡	0·05	0·09	0·14	0·185	0·079	0·140
	(1·00)	(0·034)	(0·05)	(0·05)	(0·002)	(0·007)
Fibre§	0·045	0·095	0·135	0·185	0·06	0·17
Fibre‖				0·188	0·045	0·145
					0·093	

The positions of the 1st layer line maxima E and F were estimated from their solution scattering vectors **S** (Table 1) by triangulation, employing a spacing of 0·246 nm^{-1} from the equator to the 1st layer line. Numbers in parentheses are estimated relative peak intensities. All specimens were assembled from microtubule protein.

† This study.

‡ Beese *et al.*, 1987 (Fig. 1).

§ Wais-Steider *et al.*, 1987.

‖ Mandelkow *et al.*, 1977.

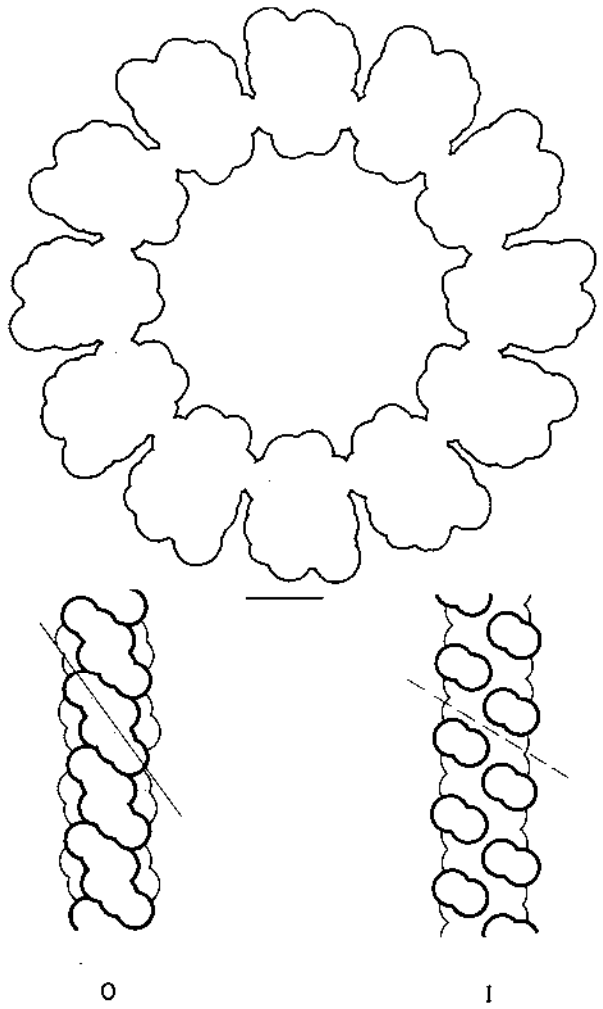

Figure 11. Schematic representation of the taxol microtubule model employed to fit the X-ray solution scattering data, shown exclusively for the purpose of discussion. In the upper part a contour end view of the model is shown. The lower part shows the contour of 1 protofilament when viewed from the outside (O) and from the inside (I) of the microtubule, with the most salient features drawn in thick lines. The bar represents 4 nm, and the model was constructed of a series of spheres of diameter 1·5 nm inside an approximately triaxial ellipsoidal envelope. The results of the fitting procedure have to be taken with caution because of the possibility of a false minimum in the minimization (see Materials and Methods, section (d)). However, there are several structural parameters derived from the modelling procedure that ought to be common to all shapes for the monomer leading to a reasonable agreement with the experimental data. The tubulin monomer must have an extension of about 7 to 8 nm in the radial direction (i.e. the width of the microtubule wall), as thicknesses of less or more than these values do not reproduce the ratio of intensities between the low angle subsidiary maxima of the J_0 Bessel function and those arising from the J_{12}, J_3 and J_9 Bessel functions (or the J_{13}, J_3 and J_{10} in a 13 protofilament microtubule). The position of the electron density grooves in the microtubule wall, giving rise to the contrast between the protofilaments, must be more prominent on the outside wall. This places the main lateral contact between the tubulin monomers towards the inside of the wall, which has less contrast in the grooves between the protofilaments. Failure to include these features of the monomer leads to wrong position and wrong relative intensity of the J_{12} scattering maximum. When viewed from the outside of the microtubule, the tubulin monomer appears to have a long axis of 7·5 to 8 nm and a ridge of density at approx. 30° relative to the microtubule axis, and a short axis of approx. 5·5 nm. Finally, the tubulin monomer, when viewed from the inside of the microtubule, must have a groove in the density running at about 65° relative to the microtubule axis and roughly dissecting the monomer in the middle. These features are necessary to obtain the relative intensities and positions of the J_3 and J_9 scattering maxima.

The well-established binding stoichiometry of one taxol molecule per tubulin dimer in the microtubule is more simply interpreted as selective binding to either α or β-tubulin. Although the different tubulin monomers cannot currently be distinguished by X-ray scattering, they could be chemically distinguished by the binding of the ligand within the microtubule lattice. However, as shown in Figure 10, a 12 protofilament 3-start lattice implies that either taxol would not bind at the microtubule closure, or that it would bind to both tubulin chains. The fact that the binding of taxol to the tubulin heterodimer is not detectable in practice within this ligand solubility limit (Takoudju *et al.*, 1988; V. Peyrot & J. M. Andreu, unpublished results) indicates that it is unlikely that taxol would bind to the heterodimer and directly induce its assembly in a simple ligand-mediated polymerization reaction. On the other hand, under conditions of insignificant spontaneous assembly, taxol rapidly induces microtubule polymerization, indicating that a simple ligand-facilitated polymer stabilization mechanism (which would be kinetically limited by the rate of spontaneous assembly) is also improbable. Hence, the favoured hypothesis is that taxol should bind to intermediate species of the assembly pathway (i.e. pre-existing tubulin Mg^{2+}-induced oligomers) and transform them into actively polymerizing species.

Analysis of the time-resolved X-ray scattering data, produced by taxol-induced assembly of purified tubulin in its GTP and GDP bound forms (to be reported elsewhere), indicates that taxol promotes the sideways accretion of longitudinal tubulin oligomers, thus forming fragments of microtubule wall that constitute polymerization nuclei, in support of the mechanisms of assembly discussed above.

We are indebted to Dr Teresa Ruiz, Brandeis University, for the micrographs of Figure 6. We thank Dr Matthew Suffness, N.C.I., N.I.H. for taxol, Dr Isabel Barasoain for the C.Al 20-5 monoclonal IgG, Dolores Guirao and Eloy Blanco for help with thin section and negative stain electron microscopy, and Aurelio Hurtado for the drawings. We also acknowledge the support received from the staff of the Daresbury Laboratory and, in particular, that from our colleagues G. R. Mant, G. Diakun, S. Slawson and J. Sheldon. This work was supported by DGICyT grant PB870220, the SERC's Synchrotron Radiation Facility Committee beam time award SP01, and travel funds from DGCIyT and CSIC.

References

Abramowitz, M. & Stegun, I. A. (1965). Editors of *Handbook of Mathematical Functions*, Dover Publications Inc., New York.

Amos, L. A. (1979). Structure of microtubules. In *Microtubules* (Roberts, K. & Hyams, J. S., eds), pp. 1–64, Adaemic Press, New York.

Amos, L. A. & Eagles, P. M. A. (1987). Microtubules. In *Fibrous Protein Structure* (Squire, J. M. & Vibert, P. J., eds), pp. 215–246, Academic Press, London.

Amos, L. A. & Klug, A. (1974). Arrangement of subunits in flagellar microtubules. *J. Cell Sci.* **14**, 523–549.

Andreu, J. M. & Timasheff, S. N. (1986). The measurement of co-operative protein self-assembly by turbidity and other techniques. *Methods Enzymol.* **130**, 47–59.

Andreu, J. M., Garcia de Ancos, J., Starling, D., Hodgkinson, J. L. & Bordas, J. (1989). A synchrotron X-ray scattering characterization of purified tubulin and of its expansion induced by mild detergent binding. *Biochemistry*, **28**, 4036–4040.

Andreu, J. M., Garcia de Ancos, J., Medrano, F. J., Gil, R., Diaz, J. F., Nogales, E., Towns-Andrews, E., Pantos, E. & Bordas, J. (1991). Twelve protofilament taxol-induced microtubules assembled from purified tubulin. *Amer. Inst. Phys. Conf. Proc.* **227**, 160–169.

Arevalo, M. A., Nieto, J. M., Andreu, D. & Andreu, J. M. (1990). Tubulin assembly probed with antibodies to synthetic peptides. *J. Mol. Biol.* **214**, 105–120.

Asnes, C. & Wilson, L. (1979). Isolation of bovine brain microtubule protein without glycerol: polymerization kinetics change during purification cycles. *Anal. Biochem.* **98**, 64–73.

Beese, L., Stubbs, G. & Cohen, C. (1987). Microtubule structure at 18 Å resolution. *J. Mol. Biol.* **194**, 257–264.

Bordas, J. (1989). Research facilities for biology at the synchrotron radiation source at Daresbury Laboratory. *Basic Life Sci.* **51**, 55–62.

Bordas, J. & Mandelkow, E. (1982). Time-resolved X-ray scattering from solutions using synchrotron radiation. In *Fast Methods in Physical Biochemistry and Cell Biology* (Sha'afi, R. I. & Fernandez, S. M., eds), pp. 137–172, Elsevier, Amsterdam.

Bordas, J., Mandelkow, E. M. & Mandelkow, E. (1983). Stages of tubulin assembly and disassembly studied by time-resolved synchrotron X-ray scattering. *J. Mol. Biol.* **164**, 89–135.

Carlier, M. F. & Pantaloni, D. (1983). Taxol effect on tubulin polymerization and associated guanosine 5′-triphosphate hydrolysis. *Biochemistry*, **22**, 4814–4822.

Chalfie, M. & Thomson, J. N. (1982). Structural and functional diversity in the neuronal microtubules of *Caenorhabditis elegans*. *J. Cell Biol.* **93**, 15–23.

Chrétien, D., Job, D. & Wade, R. H. (1990). Observations of frozen-hydrated microtubules. *Proc. XIIIth Int. Congr. Electron Microsc.* **1**, 504–505.

Collins, C. A. & Valee, R. B. (1987). Temperature-dependent reversible assembly of taxol-treated microtubules. *J. Cell Biol.* **105**, 2847–2854.

Darnell, J., Lodish, H. & Baltimore, D. (1990). *Molecular Cell Biology*, W. H. Freeman and Co., New York.

de la Viña, S., Andreu, D., Medrano, F. J., Nieto, J. M. & Andreu, J. M. (1988). Tubulin structure probed with antibodies to synthetic peptides. Mapping of three major types of limited proteolysis fragments. *Biochemistry*, **27**, 5352–5365.

Dubochet, J., Adrian, M., Jiin-Ju, C., Lepault, J. & McDowell, A. W. (1987). Cryo-electron microscopy of vitrified specimens. In *Cryotechniques in Biological Microscopy* (Steinbrecht, R. A. & Zierold, B. H., eds), pp. 114–128. Springer Verlag, Berlin, Heidelberg.

Gil, R. (1988). Cytoskeletal components of *Frontonia depressa* (Ciliophora Hymenostomatida). *Trans. Amer. Microsc. Soc.* **107**, 410–420.

Gregory, L., Davis, K. G., Sheth, B., Boyd, J., Jefferis, R., Nave, C. & Burton, D. R. (1987). The solution conformation of the subclasses of human IgG deduced from sedimentation and small angle X-ray scattering studies. *Mol. Immunol.* **24**, 821–829.

Guinier, A. & Fournet, G. (1955). *Small Angle Scattering of X-rays*, Wiley, New York.

Hamel, E., ed. (1992). Microtubule Inhibitors, *International Encyclopedia of Pharmacology and Therapeutics*, Pergamon Press, in the press.

Hernandez, M. A., Avila, J. & Andreu, J. M. (1986). Physicochemical characterization of the heat-stable microtubule-associated protein MAP2. *Eur. J. Biochem.* **154**, 41–48.

Howard, W. D. & Timasheff, S. N. (1986). GDP state of tubulin: stabilization of double rings. *Biochemistry*, **25**, 8292–8300.

Howard, W. D. & Timasheff, S. N. (1988). Linkages between the effects of taxol, colchicine, and GTP on tubulin polymerization. *J. Biol. Chem.* **263**, 1342–1346.

Klug, A., Crick, F. H. C. & Wyckhoff, H. W. (1958). Diffraction by helical structures. *Acta Crystallogr. sect.* , **11**, 199–213.

Langford, G. M. (1980). Arrangement of subunits in microtubules with 14 protofilaments. *J. Cell Biol.* **87**, 521–526.

Lee, J. C. (1982). Preparation and chemical properties of calf brain tubulin. *Methods Cell Biol.* **24**, 9–30.

Lee, J. C. & Timasheff, S. N. (1975). The reconstitution of microtubules from purified calf brain tubulin. *Biochemistry*, **14**, 5183–5187.

Lee, J. C., Frigon, R. P. & Timasheff, S. N. (1973). The chemical characterization of calf brain microtubule protein subunits. *J. Biol. Chem.* **248**, 7253–7262.

Mandelkow, E. (1986). X-ray diffraction of cytoskeletal fibres. *Methods Enzymol.* **134**, 633–657.

Mandelkow, E. & Bordas, J. (1986). Time-resolved X-ray scattering of microtubule assembly using synchrotron radiation. *Methods Enzymol.* **134**, 657–676.

Mandelkow, E., Thomas, J. & Cohen, C. (1977). Microtubule structure at low resolution by X-ray diffraction. *Proc. Nat. Acad. Sci., U.S.A.* **74**, 3370–3374.

Mandelkow, E. M., Harmsen, A., Mandelkow, E. & Bordas, J. (1980). X-ray kinetic studies of microtubule assembly using synchrotron radiation. *Nature (London)*, **287**, 595–599.

Mandelkow, E., Mandelkow, E. M. & Bordas, J. (1983). Structure of tubulin rings studied by X-ray scattering using synchrotron radiation. *J. Mol. Biol.* **167**, 179–186.

Mandelkow, E. M., Schulteiss, R., Rapp, R., Müller, M. & Mandelkow, E. (1986). On the surface lattice of microtubules: helix starts, protofilament number, seam, and handedness. *J. Cell Biol.* **102**, 1067–1073.

Marx, A., Jagla, A. & Mandelkow, E. (1990). Microtubule assembly and oscillations induced by flash photolysis of caged-GTP. *Eur. Biophys. J.* **19**, 1–9.

Mitchinson, T. & Kirschner, M. (1984). Dynamic instability of microtubule growth. *Nature (London)*, **312**, 237–242.

Mogensen, M. & Tucker, J. B. (1990). Taxol influences control of protofilament number at microtubule-nucleating sites in *Drosophila*. *J. Cell Sci.* **97**, 101–107.

Na, G. C. & Timasheff, S. N. (1981*a*). Interaction of calf brain tubulin with glycerol. *J. Mol. Biol.* **151**, 165–178.

Na, G. C. & Timasheff, S. N. (1981*b*). Physical properties of purified calf brain tubulin. *Methods Enzymol.* **85**, 393–408.

Oosawa, F. & Asakura, S. (1975). *Thermodynamics of the Polymerization of Protein*, Academic Press, London.

Pantos, E., Mant, G. R., Starling, D., Jones, G. R. & Bordas, J. (1988). Three dimensional structure simulation: application to electron microscopy and X-ray diffraction data. In *Proc. 2nd International Conference on Biophysics and Synchrotron Radiation, Chester*, pp. 205–208, Daresbury Laboratory.

Parness, J. & Horwitz, S. B. (1981). Taxol binds to polymerized tubulin *in vitro*. *J. Cell Biol.* **91**, 479–487.

Ringel, I. & Horwitz, S. B. (1991). Effect of alkaline pH on taxol-microtubule interactions. *J. Pharm. Exp. Ther.* **259**, 855–860.

Rowinsky, E. K., Cazenave, L. A. & Donehower, R. C. (1990). Taxol: a novel investigational anti-microtubule agent. *J. Nat. Cancer Inst.* **82**, 1247–1259.

Schiff, P. B. & Horwitz, S. B. (1981). Taxol assembles tubulin in the absence of exogenous guanosine. *Biochemistry*, **20**, 3247–3252.

Schiff, P. B., Fant, J. & Horwitz, S. B. (1979). Promotion of microtubule assembly *in vitro* by taxol. *Nature (London)*, **277**, 665–667.

Slaughter, C. A., Siegelman, M., Estess, P., Barasoain, I., Nisonoff, A. & Capra, D. (1982). Antibody diversity and idiotypes: primary structural analysis of monoclonal A/J anti-arsonate antibodies. In *Developmental Immunology: Clinical Problems and Aging* (Cooper, E. L. & Brazier, M. A. B., eds), pp. 45–68, Academic Press, New York.

Spann, U., Renner, W., Mandelkow, E. M., Bordas, J. & Mandelkow, E. (1987). Tubulin oligomers and microtubule assembly studied by time-resolved X-ray scattering: separation of prenucleation and nucleation events. *Biochemistry*, **26**, 1123–1132.

Takoudju, M., Wright, M., Chenu, J., Gueritte-Voelgelein, F. & Guenard, D. (1988). Absence of 7-acetyl taxol binding to unassembled brain tubulin. *FEBS Letters*, **227**, 96–98.

Taylor, E. W. (1965). The mechanism of colchicine inhibition of mitosis. *J. Cell Biol.* **25**, 145–160.

Taylor, K. A. & Glaeser, R. M. (1976). Electron microscopy of frozen hydrated biological specimens. *J. Ultrastruct. Res.* **55**, 448–456.

Tilney, L. G., Brian, J., Bush, D. J., Fujiwara, K., Mooseker, M. S., Murphy, D. B. & Snyder, D. H. (1973). Microtubules: evidence for 13 protofilaments. *J. Cell Biol.* **59**, 267–275.

Towns-Andrews, E., Berry, A., Bordas, J., Mant, G. R., Murray, P. K., Roberts, K., Sumner, I., Worgan, J. S., Lewis, R. & Gabriel, A. (1989). A time-resolved X-ray diffraction station: X-ray optics, detectors and data acquisition. *Rev. Sci. Instrum.* **60**, 2346–2349.

Vallee, R. B. (1980). Structure and phosphorylation of microtubule-associated protein 2 (MAP2). *Proc. Nat. Acad. Sci., U.S.A.* **77**, 3206–3210.

Vibert, P. J. (1987). Fibre diffraction methods. In *Fibrous Protein Structure* (Squire, J. M. & Vibert, P. J., eds), pp. 23–45, Academic Press, London.

Wade, R. H., Pirollet, F., Margolis, R. L., Garel, J. R. & Job, D. (1989). Monotonic *versus* oscillating microtubule assembly: a cryo-electron microscope study. *Biol. Cell*, **65**, 37–44.

Wade, R. H., Chrétien, D. & Job, D. (1990). Characterization of microtubule protofilament numbers. How does the surface lattice accommodate? *J. Mol. Biol.* **212**, 775–786.

Wade, R. H., Chrétien, D. & Pantos, E. (1991). Concerning the surface lattice of microtubules. In *Electron Crystallography, Proceedings of NATO Workshop*, Erice, Italy (Fryer, J. R. & Dorset, D. L., eds), pp. 317–325, Kluwer, Dordrecht, The Netherlands.

Wais-Steider, C., White, N. S., Gilbert, D. S. & Eagles, P. A. M. (1987). X-ray diffraction patterns from microtubules and neurofilaments in axoplasm. *J. Mol. Biol.* **197**, 205–218.

Wani, M. C., Taylor, H. L., Wall, M. E., Coggon, P. & McPhail, A. T. (1971). Plant antitumour agents. VI. The isolation and structure of taxol, a novel anti-leukemic and antitumour agent from *Taxus brevifolia*. *J. Amer. Chem. Soc.* **93**, 2325–2327.

Weisenberg, R. C., Borisy, G. G. & Taylor, E. (1968). The colchicine-binding protein of mammalian brain and its relation to microtubules. *Biochemistry*, **7**, 4466–4479.

Williams, R. C. & Rone, L. A. (1989). End-to-end joining of taxol-stabilized GDP-containing microtubules. *J. Biol. Chem.* **264**, 1663–1670.

Wilson, L., Miller, H. P., Farrell, K. W., Snyder, K. B., Thompson, W. C. & Purich, D. L. (1985). Taxol stabilization of microtubules *in vitro*: dynamics of tubulin addition and loss at opposite microtubule ends. *Biochemistry*, **24**, 5254–5262.

Woody, R. W., Clark, D. C., Roberts, G. C., Martin, S. & Bayley, P. M. (1983). Molecular flexibility in microtubule proteins: proton nuclear magnetic resonance characterization. *Biochemistry*, **22**, 2186–2192.

Edited by V. Luzzati